

Solution of population balance equations by logarithmic shape preserving interpolation on finite elements

Liborio I. Costa

Etzbergstrasse 19c, 8405, Winterthur, Switzerland

Giuseppe Storti

ETH Zurich, Vladimir-Prelog-Weg 1, 8093, Zurich, Switzerland

Stefano Lazzari

Massachusetts Institute of Technology, 77, Massachusetts Avenue, 02139 Cambridge, MA, USA

Abstract

A new numerical approach for solving population balance equations (PBE) is proposed and validated. The method employs a combination of basis functions, defined on finite elements, to approximate the sought distribution function. Similarly to other methods of the same family, the PBE are solved only in a finite number of values of the internal coordinate (grid points). The peculiarity of the method is the use of a logarithmic, shape-preserving interpolation (LSPI) procedure to estimate the values of the distribution in between grid points. The main advantages of the LSPI method compared to other approaches of the same category are: i) the stability of the numerical approach (*i.e.* the absence of oscillations in the distribution function occurring when using “standard” cubic splines and a low number of elements), and ii) the conceptual and implementation simplicity, as no mathematical manipulation of the PBE is required.

Keywords: Population balance equations, Aggregation, Breakage, Finite elements, Interpolation

1. Introduction

The synthesis of new materials and the continuous technological progress allowed an impressive advancement in different fields, leading to the realization of new types of drugs, more efficient solar panels, electronics and plastics derived from renewable resources. Most of these materials are synthesized through an assembly process of subunits (molecules or particles) that typically form differently sized assemblies, rather than one-sized structures.[1, 2, 3, 4, 5, 6] To properly control and optimize these assembly processes, a mathematical framework is of indisputable importance. For this reason, the differential equation set, known as population balance equations (PBE), has been used extensively since its formal introduction.[7, 8]

PBE have been employed to rationalize polymerization reactions [9, 10, 11, 12, 13, 14, 15, 16, 17, 18, 19, 20, 21], colloid aggregation, [22, 23, 3, 24, 25, 26, 27, 28] and crystallization processes[29, 30, 31, 32, 33]. This short list proves the versatility of the PBE, that enable the description of virtually any type of population, focusing on some key property such as the number of monomeric units in polymer chains, or the size of crystals. These properties, usually referred to as the internal coordinates of the PBE, define the discrete (*e.g.* the number of monomers) or continuous nature (*e.g.* the length of a crystal) of the PBE.

Whether discrete or continuous, the PBE can be solved either with stochastic or deterministic approaches.[8] Stochastic methods are indeed very interesting and may reveal structural and topological information of the assemblies, but their lengthy computational times make them unsuitable to be employed for process optimization.[18, 8] Deterministic approaches overcome this hurdle and allow the quantification of kinetic rates. An overview of the available deterministic strategies to solve the PBE is discussed in the following, considering a one dimensional distribution function in its continuous formulation. These considerations equally apply to discrete balances and multidimensional PBE, although the latter remain out of the scope of the present paper. For this general considerations, we will refer to $f(x, t)dx$, representing the number concentration of species (*i.e.* clusters, chains, aggregates), consisting of x to $x + dx$ units.

The first class of methods to be historically proposed, is based on the integral properties of the distribution, the so called “moments”.[7] By focusing only on the moments of the distribution, the method delivers results by integrating only a few ordinary differential equations. The price to pay is

38 threefold: i) the need of assuming a distribution shape in order to reconstruct
39 the size distribution $f(x, t)$, ii) the lack of generality (some mass-dependent
40 rate equations cannot be easily employed), and iii) the necessity of often hav-
41 ing to employ closure equations.[34, 35] Nevertheless, the method of moments
42 has been proven very powerful in dealing with multidimensional and complex
43 balances, for instance in the case of non-linear polymerizations.[11, 18]

44 An improvement of the method of moments is represented by the quadra-
45 ture method of moments (QMOM) and its variations.[28, 35] By solving a
46 few more differential equations (usually 6-12), these approaches still suffer of
47 the necessity of assuming a distribution shape when reconstructing $f(x, t)$,
48 but overcome the remaining issues of the method of moments. Providing av-
49 erage properties accurately and with little computational power, enabled the
50 method of moments and the QMOM to solve PBE in spatially distributed
51 systems[36] and in computational fluid dynamic frameworks.[28, 35]

52 When interested in obtaining the full distribution $f(x, t)$ without making
53 assumptions regarding its shape, other approaches such as i) the method of
54 generating functions, ii) finite differences schemes, iii) the method of dis-
55 cretized PBEs, and iv) the method of basis functions can be used.

56 The generating function method[37, 38] relies on solving the PBE in the
57 Laplace space and then inverting the solution to re-obtain the desired dis-
58 tribution. This inversion step is numerical in most cases and represents the
59 main drawback of the generating functions approach, given the related nu-
60 merical complexities.[9]

61 In the “finite differences” approach, both the time and the internal co-
62 ordinate domain are discretized, replacing all derivatives in the PBE with
63 finite differences. To this class belong also the high resolution finite vol-
64 ume methods, that employ higher-order approximation of the derivatives.
65 These latter methods reduce the numerical diffusion problems often encoun-
66 tered by “standard” finite difference approaches in nucleation and growth
67 problems.[39, 40] Nevertheless, these methods are computationally demand-
68 ing when aggregation and breakage are of interest, because of the quite fine
69 grids usually required to obtain accurate results.[41]

70 Discretized PBE methods, or method of classes or sectional methods, rely
71 on the subdivision of the internal coordinate in a number of finite, continuous,
72 intervals (or bins). [42, 43, 44, 15, 45] The representative values of the internal
73 coordinate within each bin are referred to as pivotal values. The PBE are re-
74 written accounting for each pivotal value, imposing the preservation of one or
75 more properties of the distribution.[42, 46] For example, whenever a cluster is

76 formed whose mass does not correspond to a pivotal value, it is redistributed
77 among the nearest pivots in order to preserve the first two moments of the
78 distribution. The discretized PBE are one of the most applied methods,
79 especially since the formulation due to Kumar and Ramkrishna.[42] Despite
80 the constant improvement throughout the years,[46, 47, 45] the method may
81 suffer of some inaccuracies in predicting higher order moments when a low
82 number of pivots is used, and it is not of straightforward use because of the
83 rather complex mathematical treatment necessary to implement and apply
84 the methodology.

85 Another class of methods approximates the unknown distribution $f(x, t)$
86 using a set of known basis functions $\phi_i(x)$ multiplied by weighting coefficients
87 $a_i(t)$, where $i = 1, 2, \dots, N$, with N being the total number of basis functions
88 employed. Within this category different sub-methods can be distinguished,
89 according to a) the domain in which the basis functions $\phi_i(x)$ are defined, b)
90 the specific form of the selected basis functions $\phi_i(x)$, and c) the way the co-
91 efficients $a_i(t)$ are determined. When the basis functions $\phi_i(x)$ are defined on
92 intervals (e.g. when piecewise polynomials are used to approximate $f(x, t)$)
93 one speaks of basis function on finite elements,[48, 49, 50] otherwise, one
94 refers to spectral basis functions.[51, 52] The choice of the basis function is key
95 in this method, as it determines its stability and accuracy.[49] Many different
96 functions have been tested to this end, ranging from linear functions,[49] to
97 different cubic polynomials,[48, 53, 43] or Gaussian functions.[52] A further
98 distinction among these methods is related to how the unknown coefficients
99 (or weights) $a_i(t)$ are determined.[54] The “method of the weighted residuals”
100 is one of the most popular for determining such coefficients.[48, 53, 51, 54]
101 Here, the approximated form of the solution is substituted in the PBE thus
102 giving a formulation of the residual function, which needs to be minimized.
103 Depending on the minimization strategy, one obtains different formulations
104 of the weighted residual method, such as the Galerkin or the collocation
105 method. In a few other cases, no minimization of the residual is performed,
106 and the coefficients are obtained “directly” by using C^2 cubic splines,[55] by
107 solving an algebraic[48] or a differential equation system.[52]

108 In this frame, the present work introduces a new numerical approach
109 that falls in the category of the basis functions method on finite elements
110 (*i.e.* the basis functions are defined on intervals). Instead of considering
111 $f(x, t)$, we approximate its natural logarithm, $\ln(f(x, t))$, using a cubic poly-
112 nomial: $\ln(f(x, t)) \approx a_i(t)x^3 + b_i(t)x^2 + c_i(t)x + d_i(t)$, where i represents the
113 i^{th} interval considered. This implies that the $f(x, t)$ is approximated in each

114 interval i with an exponential function: $f(x, t) \approx e^{a_i(t)x^3 + b_i(t)x^2 + c_i(t)x + d_i(t)}$.
 115 Notably, Hermite shape-preserving cubics are considered to approximate the
 116 $\ln(f(x, t))$, implying that the determination of the time-dependent coeffi-
 117 cients (a_i, b_i, c_i, d_i) is direct and bypasses the calculation of a residual. The
 118 main advantages of the logarithmic shape preserving interpolation (LSPI)
 119 method are i) that no mathematical manipulation of the original PBEs is
 120 required, resulting in a simple numerical implementation when compared to
 121 other approaches,[54, 42, 40] and ii) the stability and accuracy of the method
 122 even when using a low number of elements compared to similar approaches
 123 relying on low-order polynomials.[48, 49] By using a shape preserving interpo-
 124 lation, in fact, the oscillations often encountered when applying polynomial
 125 interpolations on sparse grids [56] are automatically avoided.

126 The work is structured as follows. First the LSPI method is presented
 127 and then validated employing aggregation and breakage mechanisms, using
 128 both discrete and continuous PBE. Initially, a purely aggregating system
 129 is considered and the LSPI predictions are compared with analytical solu-
 130 tions of the PBE using three different kernels (constant, sum, and prod-
 131 uct). Then a comparison with an accepted literature approach relying on
 132 Gaussian basis functions,[52] is carried out to validate the LSPI approach
 133 with diffusion-limited, and reaction-limited aggregation. Finally, the LSPI
 134 method is validated in the frame of aggregating-breaking systems. To this
 135 end, a random breakage kernel resulting in an analytical solution was em-
 136 ployed. To test the LSPI approach also with non-analytical breakage prob-
 137 lems, mass- and position-dependent breakage kernels have been selected and
 138 the LSPI solutions were compared with the aforementioned literature numer-
 139 ical approach.[52]

140 **2. Logarithmic shape-preserving interpolation - numerical and math-** 141 **ematical aspects**

142 The logarithmic shape-preserving interpolation (LSPI) method is pre-
 143 sented in this section. For the sake of clarity, the method is introduced for
 144 systems undergoing aggregation only, for both the continuous (Section 2.1)
 145 and the discrete (Section 2.2) formulations of the PBE. The straightforward
 146 generalization to the case of aggregation/breakage is shortly discussed in Sec-
 147 tion 3, while a complete list of symbols is provided in the appendix in Tables
 148 4 and 5.

149 *2.1. Logarithmic shape-preserving interpolation - continuous PBE*

150 To illustrate the method, let us first consider the PBE for a system un-
 151 dergoing aggregation only:

$$\begin{aligned} \frac{\partial f(x, t)}{\partial t} = & - f(x, t) \int_0^\infty \beta(x, y) f(y, t) dy \\ & + \int_0^{x/2} \beta(x - y, y) f(x - y, t) f(y, t) dy \end{aligned} \quad (1)$$

152 where $f(x, t)$ is the population density (or distribution function), and $f(x, t)dx$
 153 represents the number concentration of clusters at time t with size comprised
 154 between x and $x + dx$. $\beta(x, y)$ is the aggregation kernel, describing the rate of
 155 combination of two clusters, of sizes x and y . Note that x and y will be used
 156 along the text to indicate the sizes or masses of the clusters, hence they do
 157 refer to the same internal coordinate of the distribution function. The first
 158 term in equation 1 represents the rate of disappearance of the clusters of size
 159 x due to their aggregation with other clusters (of any size). The second term,
 160 i.e. the convolution integral, represents the formation rate of an aggregate
 161 of size x from the aggregation of smaller clusters.

162 The LSPI approach provides a solution for the PBE (equation 1) employ-
 163 ing a 4-step procedure:

- 164 (i) The continuous PBE is written for a number I of grid points x_i , where
 165 $i = 1, 2, \dots, I$, obtaining the corresponding I ordinary differential equa-
 166 tions:

$$\begin{aligned} \frac{df(x_i, t)}{dt} = & - f(x_i, t) \int_{x_{min}}^{x_{max}} \beta(x_i, y) f(y, t) dy \\ & + \int_{x_{min}}^{x_i/2} \beta(x_i - y, y) f(x_i - y, t) f(y, t) dy \end{aligned} \quad (2)$$

167 Here, $x_1 = x_{min}$ and $x_I = x_{max}$ represent the minimum and maximum
 168 values of the internal coordinate used for the numerical solution. Note
 169 that the I grid points x_i define the boundaries of the $I - 1$ finite elements
 170 in which the domain of x is subdivided.

- 171 (ii) Each distribution function appearing in the integrals is interpolated on
 172 J knots y_j , with $j = 1, 2, \dots, J$, covering the full integration domain.
 173 With reference to equation 2, this corresponds to obtaining the values

174 $f(y_j, t)$ with $y_1 = x_{min}$ and $y_J = x_{max}$ for the first integral, as well
175 as $f(x_i - y_j, t)$ and $f(y_j, t)$ with $y_1 = x_{min}$ and $y_J = x_i/2$ for the
176 convolution integral.

177 (iii) The integrals in equation 2 are numerically evaluated using the J knots
178 of point ii), relying on standard quadrature approaches.

179 (iv) The I time derivatives of $f(x_i, t)$ in equation 2 are calculated, and a
180 time integration step is performed. Steps ii) and iii) are then repeated
181 iteratively at each integration time step.

182 In the following, the two key steps of the LSPI method, interpolation and
183 numerical integration, will be discussed, highlighting the differences of the
184 LSPI approach compared to other methods using basis functions on finite
185 elements.

186 2.1.1. Interpolation

187 In the context of PBE, the main requirements for an effective interpolant
188 are:

- 189 (i) it approximates well the shape of the function $f(x, t)$ over the whole
190 domain of the independent variable x ;
- 191 (ii) it can be computed easily and efficiently;
- 192 (iii) it preserves the non-negativity of $f(x, t)$;
- 193 (iv) it requires a low number of interpolating points.

194 Hermite shape preserving cubic polynomials fulfill all the above requirements
195 and do not need any a-priori knowledge of the shape of the function to be
196 interpolated.[57, 58] Moreover, they are relatively straightforward to com-
197 pute.

198 Unlike other methods which use (non-shape preserving) C^1 cubic inter-
199 polants, they do not require the definition of additional points (collocation
200 points) within each finite elements where the residual of the differential
201 equation has to be minimized in order to determine the coefficients of the
202 interpolant.[48, 53, 58, 27] In our case, the cubic coefficients are obtained
203 directly from a step by step approach once the coordinates $(x_i, f(x_i, t))$ are
204 known without any need to solve for large algebraic or algebraic-differential
205 systems. Additionally, they are also free from the oscillations and overshoot-
206 ings that may arise when using C^2 cubic splines and only a few interpolation
207 points.[58, 56]

208 Recalling that at each time t we know the values of the distribution
209 function in the I grid points x_i , using a shape preserving Hermite polynomial

210 implies that $(I - 1)$ cubic interpolants $P(y, t)$ will be used, one for each of
 211 the $(I - 1)$ elements.

212 In order to limit the number of elements required to approximate $f(x, t)$,
 213 it is useful recalling that for aggregating systems the population density
 214 $f(x, t)$ is often of exponential nature [48, 59]. Therefore, one can infer that
 215 the same interpolation accuracy may be achieved with fewer grid points when
 216 interpolating the logarithm of the density function rather than the density
 217 function itself. In other words, instead of using $f(x_i, t)$, we will use the values
 218 $\ln(f(x_i, t))$ to carry out the interpolation.

219 Employing the $\ln(f(x_i, t))$ comes with a *caveat*. Although the popula-
 220 tion density is non-negative in the whole domain by definition, numerical
 221 errors may arise when integrating equation 2, as in any other approximated
 222 approach, leading the $f(x_i, t)$ values to be negative in some points, thus
 223 precluding the logarithmic transformation. This may occur during the time
 224 integration when the population decays rapidly and has extremely low values.
 225 Therefore, we define a local shift factor ϵ :

$$\epsilon = (1 + d_\epsilon) |\min\{f(x_i, t) \setminus \{0\}\}| \quad (3)$$

226 with $d_\epsilon > 0$. The local shift factor ϵ is a positive number whose value
 227 is larger (by a factor $(1 + d_\epsilon)$) than the modulus of the minimum of the
 228 non-zero elements of $f(x_i, t)$. Accordingly, whatever the values of the pop-
 229 ulation density at the grid points, $f(x_i, t) + \epsilon$ is always positive, and one
 230 can safely apply the shape preserving cubic splines using the known coordi-
 231 nates $(x_i, \ln(f(x_i, t) + \epsilon))$, from which the piecewise cubic interpolant $P(y, t)$
 232 can easily be obtained. With this in mind the sought interpolating func-
 233 tions, satisfying the above mentioned conditions and referring to the interval
 234 $h_i = [x_i \leq y < x_{i+1}]$, will have the form:

$$\begin{aligned} P(y, t) = & \ln(f(x_i, t) + \epsilon) + (y - x_i)d_i \\ & + (y - x_i)^2c_i + (y - x_i)^3b_i \end{aligned} \quad (4)$$

where $x_i \leq y < x_{i+1}$
 and $i = 1, 2, \dots, I - 1$

235 The parameters b_i, c_i and d_i required to obtain the shape-preserving inter-
 236 polant are obtained through a well-established procedure by Fritsch and
 237 Carlson, [58, 57] reported in the ESI (Section S1).

238 Equation 4 gives access to the value of the population density $f(y, t)$ at
 239 a desired coordinate y by a simple inversion:

$$f(y, t) = \exp(P(y, t)) - \epsilon \quad (5)$$

240 A synoptic view of the interpolation procedure is illustrated in Figure 1.
 241 From the known coordinates at time t , $f(x_i, t)$, one determines the minimum
 242 of the non-zero $f(x_i, t)$ values (equation 3 and Figure 1a), from which the shift
 243 factor ϵ is calculated (equation 3). This allows the calculation of $\ln(f(x_i, t) +$
 244 $\epsilon)$. Then the coefficients of the cubic interpolant (b_i, c_i, d_i) are determined
 245 in interval h_i (ESI, Section S1) for the set of points $(x_i, \ln(f(x_i, t) + \epsilon))$, as
 246 shown in Figure 1b). This interpolation procedure is repeated for all the
 247 $I - 1$ intervals, hence the logarithm of the shifted function can be evaluated
 248 at any value y_j (equation 4 and Figure 1c)). Finally, the density function
 249 itself is obtained through equation 5 (Figure 1d)).

250 2.1.2. Quadrature

251 After having interpolated using the known I points and having calculated
 252 the distribution function in all selected knots, it is possible to numerically
 253 evaluate the integrals in equation 2. Since numerical integration methods
 254 are well-known,[60] we report the corresponding details in the ESI (Section
 255 S2), while the most relevant observations on the quadrature method used are
 256 summarized here:

- 257 (i) the coordinates of the J knots for the quadrature are defined independ-
 258 dently from the I grid points x_i , decoupling the number of ordinary
 259 differential equations to be solved (I), from the appropriate number of
 260 points to perform the numerical integration;
- 261 (ii) The same number of J knots is used for the quadrature of all the PBE
 262 integrals (equation 2). Although not strictly necessary, this choice limits
 263 to a minimum the parameters of the method;
- 264 (iii) Logarithmic abscissas and higher order quadrature rules lead to a better
 265 accuracy than linear abscissas or simple trapezoidal integration (ESI,
 266 Section S2). Nevertheless, all quadrature methods converge to the
 267 same results when using a large enough number of interpolating knots,
 268 $J \approx 10^2$, confirming that any quadrature approach could be used. We
 269 used the 4th degree Newton-Cotes formulas (Boole's rule)[60] using a
 270 logarithmic scale for the integration variable, because it provided high
 271 accuracy with limited knots number (ESI, Section S2).

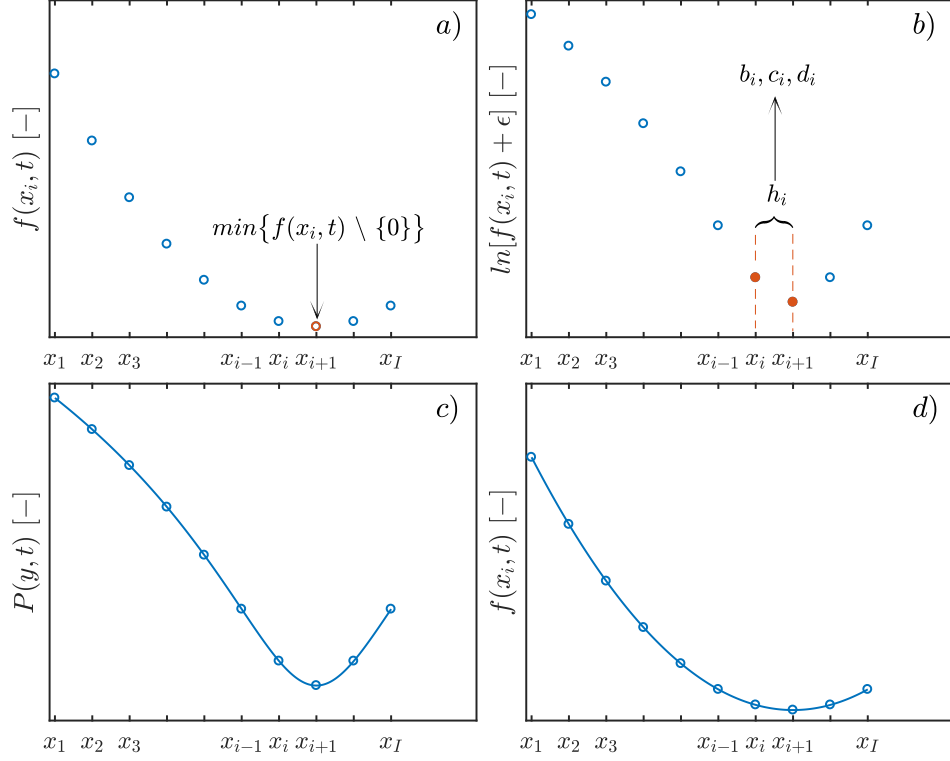


Figure 1: Scheme illustrating the interpolation procedure. In particular: a) find the minimum of $f(x_i, t)$, and compute ϵ with equation 3; b) compute $\ln(f(x_i, t) + \epsilon)$ and the coefficients of the shape preserving cubic spline (b_i, c_i, d_i) in the interval h_i (equation 4 and ESI Section S1), repeat for all intervals $I - 1$; c) use the obtained coefficients and the interpolant function $P(y, t)$ to estimate the function at selected y values (equation 4; d) convert the found values $P(y, t)$ to $f(y, t)$ using equation 5.

272 *2.2. Logarithmic interpolation - discrete PBE*

273 In the case of discrete PBE, the balance for an aggregating system be-
 274 comes:

$$\begin{aligned} \frac{df(x,t)}{dt} = & - f(x,t) \sum_{y=1}^{\infty} \beta(x,y)f(y,t) \\ & + \frac{1}{2} \sum_{y=1}^{x-1} \beta(x-y,y)f(x-y,t)f(x,t) \end{aligned} \quad (6)$$

275 Here $f(x,t)$ denotes the number concentration of the clusters with size x .
 276 Note that, in the case of discrete populations, $f(x,t)$ does not represent
 277 a density distribution, but the number (or concentration) of species with
 278 internal coordinate $x \in \mathbb{N}$, and $f(x,t)$ is defined only on the points $x \in \mathbb{N}$.
 279 To use the LSPI approach also for discrete PBEs, we write the PBEs for a
 280 finite number I of grid points x_i , and replace the summations with integrals
 281 using the Euler-Maclaurin approximation. Combining these two steps, one
 282 gets:

$$\begin{aligned} \frac{df(x_i,t)}{dt} \approx & - f(x_i,t) \left[\frac{m_i(1)}{2} + \int_1^{x_{max}} m_i(y)dy + \frac{m_i(J)}{2} \right] \\ & + \left[\frac{n_i(1)}{2} + \int_1^{\lfloor x_i/2 \rfloor} n_i(y)dy + \theta_{x_i} \frac{n_i(y_J)}{2} \right] \end{aligned} \quad (7)$$

283 The integrand functions $m_i(y)$ and $n_i(y)$ are continuous functions approxi-
 284 mating the sequences to be summed up in equation 6, for which the time-
 285 dependency has been dropped for the sake of brevity:

$$m_i(y) = \beta(x_i, y)f(y, t) \quad (8)$$

286

$$n_i(y) = \beta(x_i - y, y)f(x_i - y, t)f(y, t) \quad (9)$$

$\lfloor x_i/2 \rfloor$ represents the floor of $x_i/2$ and $\theta_{x_i} = x_i \bmod 2$:

$$\theta_{x_i} = \begin{cases} 1, & \text{if } x_i \text{ is odd} \\ 0, & \text{if } x_i \text{ is even} \end{cases} \quad (10)$$

287 Note that equation 7 implies that the summations in equation 6 are replaced
 288 by integrals plus two terms for each summation which add half of the extreme

289 values of the integrals, according to the Euler-Maclaurin approximation. In
 290 other words, although in the discrete case $f(x, t)$ has physical meaning only
 291 on the points $x_i \in \mathbb{N}$, by means of the Euler-Maclaurin approximation we can
 292 solve the discrete PBE in equation 6 by applying the very same methodology
 293 used for solving the continuous PBE to equation 7. The integrand functions
 294 are evaluated on J knots by interpolation of the I known distribution values
 295 $f(x_i, t)$, and the integrals are numerically evaluated. In the following, test
 296 cases are illustrated to validate the method.

297 3. Validation

298 In the present section the LSPI method is validated in different scenarios.
 299 The results are reported using the non-dimensional time τ defined as: [48, 59]

$$\tau = \beta(1, 1)\mu_0(t = 0)t \quad (11)$$

300 where $\mu_0(t = 0) = \int_0^\infty f(x, t = 0)dx$ is the moment of order 0, i.e. the total
 301 particle concentration, at time zero, and $\beta(1, 1)$ is the rate of aggregation of
 302 two primary particles. The LSPI method was implemented in Matlab and
 303 the PBEs were solved on a PC with 6 cores and processor AMD Phenom
 304 2.7 GHz. The system of ordinary differential equations was integrated using
 305 standard built-in ODE solvers. Unless otherwise stated, $d_\epsilon = 10^{-3}$ (equation
 306 3) and an explicit Runge-Kutta (4,5) solver with a relative tolerance of 10^{-6}
 307 and absolute tolerance of 10^{-20} were used.

308 3.1. Continuous PBE - constant and sum kernel

309 Initially, the LSPI approach is validated using continuous PBE in the
 310 frame of an aggregation problem using the constant and sum kernels. In
 311 these scenarios, analytical solutions of the PBE were available and could be
 312 compared with the numerical results of the LSPI method. The employed
 313 parameter values are reported in Table 1, and the results in Figure 2.

314 In Figure 2, the continuous black lines represent the analytical solution,
 315 the empty red circles the I grid points employed (i.e. the number of solved
 316 equations), and the red dashed lines the interpolated numerical solution.
 317 Panel a) shows a very good superimposition between numerical and analytical
 318 distributions when employing the constant kernel. Notably, panel b) reports
 319 the very same distributions as in a), plotted on a logarithmic axis in order to
 320 appreciate the performance of the numerical solution, that overlaps with the

Parameters	Constant kernel	Sum kernel
$\beta(x, y)$	1	$(x + y)$
$[x_{min}, x_{max}]$	$[10^{-3}, 500]$	$[10^{-3}, 10^4]$
Initial condition	$f(x, 0) = \frac{N_0}{x_0} e^{-\frac{x}{x_0}}$	$f(x, 0) = \frac{N_0}{x_0} e^{-\frac{x}{x_0}}$
Simulated τ [-]	$[0 - 10]$	$[0 - 4]$
$I[-]$	3	15
$J[-]$	81	81

Table 1: Kernel and parameters for the solution of continuous PBE, Figure 2. For the initial conditions, $N_0 = x_0 = 1$ were used. Analytical solutions are available in [48]

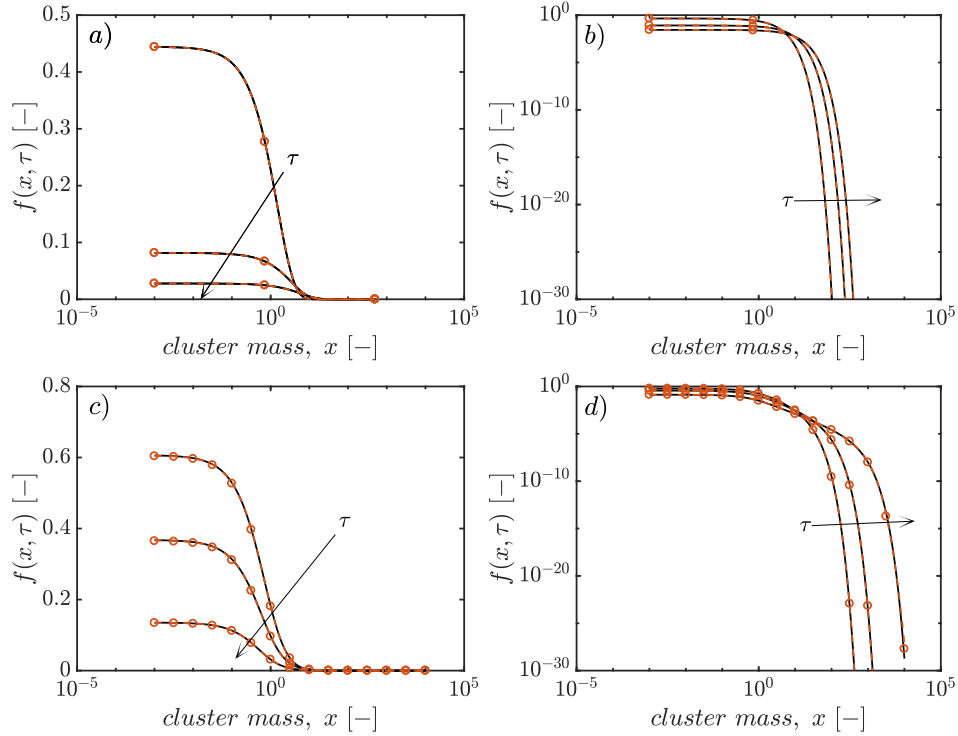


Figure 2: Time evolution of the population density for pure aggregation: LSPI solution (red) and analytical solution (black). Constant kernel, with a) linear and b) logarithmic representation of the y -axis (at $\tau = 1, 5, 10$). Sum kernel, with c) linear and d) logarithmic representation of the y -axis (at $\tau = 1, 2, 4$).

321 analytical one for 30 orders of magnitude (odm) on the y-axis and covering 6
 322 odm on the x-axis. Similar considerations hold when inspecting Figure 2 c)
 323 and d), that show distributions obtained with the sum kernel. Once again,
 324 a very good overlap of the numerical and analytical solution is observed
 325 both when plotting the results on a linear (panel c)) and logarithmic axis
 326 (panel d)). The LSPI approach guarantees in both cases highly accurate
 327 solutions using a very low number of grid points and, therefore, of differential
 328 equations to be solved. In particular, $I = 3$ for the constant kernel and
 329 $I = 15$ for the sum kernel, while in both cases $J = 81$ interpolating knots
 330 were used to compute the integrals in equation 2. The very low number of
 331 grid points used with the constant kernel is consequential to the logarithmic
 332 interpolation strategy: starting with an exponential initial condition, the
 333 exponential profile is preserved as the time increases and only three grid
 334 points (and thus three differential equations) suffice to interpolate $f(x, t)$
 335 (Figure 2 a) and b)).

336 We have further proven that the logarithmic interpolation strategy is key
 337 for obtaining accurate results even when using very few elements. This is
 338 shown for the sum kernel in the ESI (Figure S4 a) and b)) where solutions
 339 obtained with and without employing the logarithm of the distribution func-
 340 tion for the interpolation are shown. While the LSPI method superimposes
 341 with the analytical solution already with $I = 15$, the same occurs with a
 342 “standard” shape-preserving interpolation (SPI) only when using $I = 45$,
 343 and even then a deviation of the SPI is observed at the right tail of the
 344 distribution (cf. ESI, Figure S4b)).

345 3.2. Discrete PBE - pure aggregation

346 To test the LSPI approach in the case of discrete PBE, three further
 347 test cases have been considered (Table 2), using a) the product kernel, b)
 348 the diffusion-limited cluster aggregation (DLCA) kernel, and c) the reaction-
 349 limited cluster aggregation (RLCA) kernel. An analytical solution exists for
 350 the product kernel[59]. For the DLCA and RLCA kernels, the LSPI solution
 351 was compared against the numerical solution provided by the Gaussian basis
 352 functions (GBF) method.[52, 61, 62, 33]

353 In the discrete cases, the initial population distribution typically presents
 354 a singularity at $x_i = 1$. In such a case, it is therefore preferable to define
 355 the I grid points using a unitary spacing for the first few points, up to a
 356 given value I_c . Then, the usual exponential spacing can be used. In a similar
 357 way, the J knots are defined on a unitary spaced grid up to $j = I_c$ and

Parameters	Product kernel	DLCA kernel	RLCA kernel
$\beta(x, y)$	$2xy$	$\frac{2k_B T}{3\eta W} B(x, y)$	$\frac{2k_B T}{3\eta W} B(x, y)P(x, y)$
$B(x, y)$	-	$(x^{\frac{1}{d_f}} + y^{\frac{1}{d_f}}) \times$	$(x^{\frac{1}{d_f}} + y^{\frac{1}{d_f}}) \times$
	-	$(x^{-\frac{1}{d_f}} + y^{-\frac{1}{d_f}})$	$(x^{-\frac{1}{d_f}} + y^{-\frac{1}{d_f}})$
$P(x, y)$	-	-	$(xy)^{0.5}$
$[x_{min}, x_{max}]$	$[10^0, 5 \times 10^6]$	$[10^0, 5 \times 10^5]$	$[10^0, 5 \times 10^5]$
T [K]	-	298.15	298.15
η [Pa s]	-	8.9×10^{-4}	8.9×10^{-4}
D_p [m]	-	100×10^{-9}	100×10^{-9}
ϕ [-]	-	10^{-4}	10^{-4}
W [-]	-	1	10^4
d_f [-]	-	1.8	2.1
I.C. $f(1, 0)$	1	$\frac{6\phi}{\pi D_p^3}$	$\frac{6\phi}{\pi D_p^3}$
Simulated t [s]	-	4200s	42000s
Simulated τ [-]	0.998	-	-
I_c [-]	10	10	10
I [-]	26	26	26
J [-]	90	90	90

Table 2: Kernel and parameters for the solution of discrete PBE, Figure 3 and Figure 4. The absolute tolerance was 10^{-50} when using the product kernel, and 10^{-20} for the DLCA and RLCA kernels. The analytical solution for the product kernel is from reference [59]. Note that $f(x > 1, 0) = 0 \forall x > 1$. I indicates the total number of grid points, including I_c .

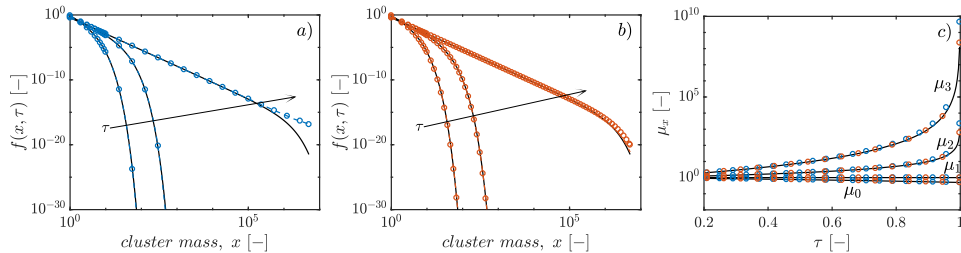


Figure 3: Discrete PBE solved for pure aggregation using the product kernel. a) and b) Distribution $f(x, \tau)$ for $\tau = \{0.2, 0.6, 0.998\}$, c) moments of order $0^{th} - 3^{rd}$ vs. τ . The analytic solutions [59] are displayed using black continuous lines. Dashed blue (with $I = 26$ and $J = 90$, (a)) and red ($I = 80$ and $J = 90$ (b)) lines are the interpolated distributions, obtained from the distribution computed at the I grid point (circles).

358 on an exponentially spaced grid (uniform on the logarithmic scale) until the
 359 upper integration limit. Accordingly, the Euler-McLaurin approximation is
 360 applied after the first $I_c - 1$ terms of the summations in Equation 6, which are
 361 summed directly. The numerical integration using Boole's rule on logarithmic
 362 abscissa coordinates was applied from $y = I_c$ to the upper integration limit.
 363 Note that, given the discrete nature of the currently considered PBE, the
 364 I grid points x_i have to be natural numbers (equation 6 and 7), while this
 365 limitation is not required for the J knots.

366 3.2.1. Product kernel - analytical solution

367 The comparisons between the results provided by the LSPI numerical
 368 method and the analytical solution of the product kernel are reported in
 369 Figure 3.

370 In particular, Figure 3 a) shows the performance of the LSPI method
 371 using $I = 26$ grid points and $J = 90$ interpolation knots. A good overlap
 372 between analytical and numerical solution is observed for the distributions
 373 at lower times, but a slight discrepancy arises for the largest τ (Figure 3a).
 374 This discrepancy vanishes as soon as the number of grid points is increased
 375 to $I = 80$, as shown in Figure 3b. It should be noted that the aforementioned
 376 discrepancy was observed at normalized concentrations as low as 10^{-20} , and
 377 only in close proximity of the gelation point,[18] ($\tau = 1$), while the agreement
 378 with the analytical solution was otherwise very good for the entire simulated
 379 time. To further prove this point the moments of order 0 to 3 (μ_0, μ_1, μ_2
 380 and μ_3) are reported against time in 3 c). In particular, the blue circles

381 represent the moments computed using $I = 26$ grid points, the red circles the
 382 solution with $I = 80$, and the continuous black lines the analytical solution.
 383 A discrepancy between the analytical solution and the LSPI method with
 384 $I = 26$ is observed only for the higher order moments at times close to the
 385 gelation of the system (typically identified when the 2nd and higher order
 386 moments diverge).[18] This further proves that even when using a very low
 387 number of grid points ($I=26$ to simulate sizes up to $5 \times 10^6!$), an accurate
 388 solution is actually obtained for practically the whole simulated time.

389 3.2.2. DLCA and RLCA aggregation

390 To verify whether the LSPI method works well also with non-analytical
 391 kernels, the DLCA and RLCA aggregation kernels have been considered.
 392 The LSPI predictions were compared with a validated literature method
 393 relying on Gaussian basis functions (GBF).[52, 61, 62] The parameter values
 394 employed for these calculations are reported in Table 2 and the results are
 395 displayed in Figure 4, where the dotted lines are the GBF solutions, while the
 396 red circles refer to the I grid points of the LSPI method. Notably, a very good
 397 overlap can be observed over 5 orders of magnitude on the abscissas and over
 398 15-20 orders of magnitude on the ordinates. When the concentrations are
 399 too low ($\approx 10^0 \# / m^3$, given an initial particle concentration of $\approx 10^{17} \# / m^3$)
 400 the GBF method starts exhibiting a 'nervousness', as already reported when
 401 the method was initially derived.[52] The LSPI method does not show any
 402 such instability, as intrinsically the method is designed to compute $f(x, t)$
 403 between the grid points with a shape-preserving cubic spline (Section 2). To
 404 further prove that the two methods are indeed performing very similarly,
 405 and that the arising discrepancy is only due to a numerical problem arising
 406 at very low concentration, the first four moments ($0^{th} - 3^{rd}$) are reported
 407 against time for the two methods for DLCA in Figure 4 c) and for RLCA
 408 in Figure 4 d). Once more, the LSPI method is represented by dashed red
 409 lines, while dotted blue lines have been employed for the GBF method. The
 410 very good overlap of the predictions, confirms that the LSPI approach is
 411 well-suited also to deal with complex kernels, such as those involved in the
 412 DLCA and RLCA aggregation mechanisms, by solving a small number of
 413 ODE. Notably, the logarithmic shape-preserving interpolation (LSPI) has
 414 been proven significantly better compared to its non-logarithmic counterpart,
 415 the shape-preserving interpolation (SPI) (ESI, Figure S4c). With the same
 416 amount of grid points $I = 26$, only the LSPI solution overlaps with the
 417 reference one provided by the GBF method, while the SPI prediction does

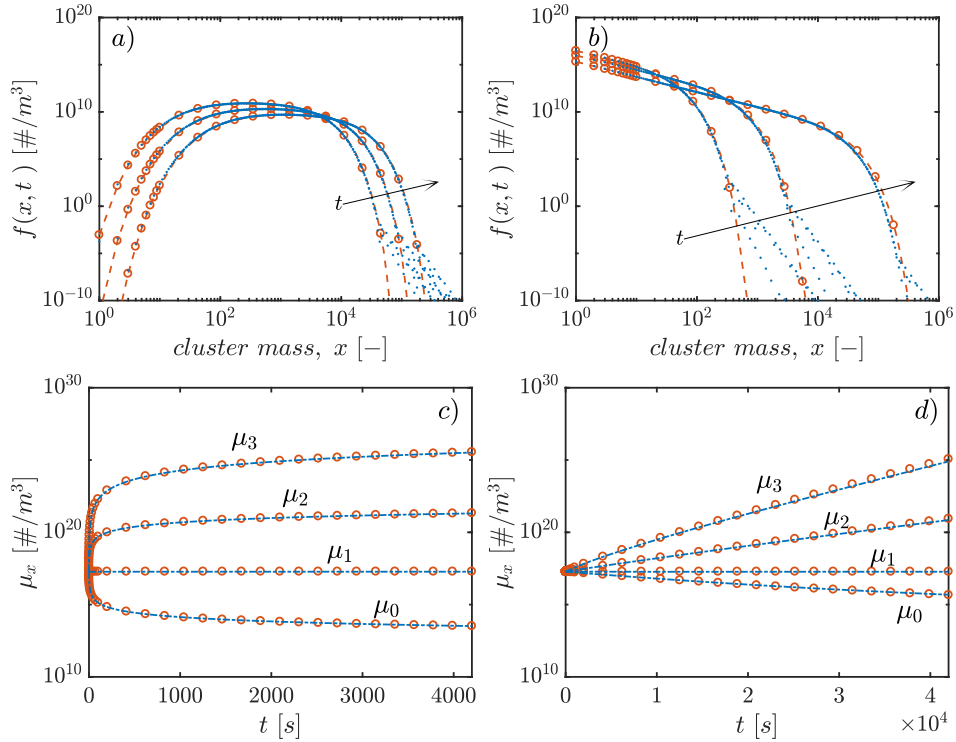


Figure 4: Discrete PBE for pure aggregation solved using a) the DLCA kernel at $\bar{t} = \{1050s, 2100s, 4200s\}$ and b) the RLCA kernel at $\bar{t} = \{10500s, 21000s, 42000s\}$. The moments of order $0^{th} - 3^{rd}$ against time are reported for c) the DLCA case, and d) the RLCA case. The blue dotted lines were obtained using the Gaussian basis functions (GBF) method, the red dashed lines with the Logarithmic shape-preserving interpolation (LSPI) method.

418 not (ESI, Figure S4c).

419 3.3. Discrete PBE - Aggregation and Breakage

420 To further prove the versatility of the proposed approach, aggregation
 421 and breakage problems have been considered as well. The general population
 422 balance accounting for aggregation and breakage reads:

$$\begin{aligned}
 \frac{df(x, t)}{dt} = & - f(x, t) \sum_{y=1}^{\infty} \beta(x, y) f(y, t) \\
 & + \frac{1}{2} \sum_{y=1}^{x-1} \beta(x-y, y) f(x-y, t) f(y, t) \\
 & - \gamma(x) f(x, t) + 2 \sum_{y=x+1}^{\infty} \Gamma(x, y) \gamma(y) f(y, t)
 \end{aligned} \tag{12}$$

423 Here $\gamma(x)$ represents the rate of breakage for the aggregate of size x , while
 424 $\Gamma(x, y)$ is the so-called daughter distribution function, representing the prob-
 425 ability that an x -sized cluster forms from the breakage of a bigger cluster
 426 of size y . The cases considered in this work rely on a parabolic daughter
 427 distribution function: [44]

$$\begin{aligned}
 \Gamma(x, y) = & \frac{0.5C}{y-1} + (1/2 - C/4) \left[\frac{8(3x^2 - 3x + 1)}{(y-1)^3} \right. \\
 & \left. - \frac{12(2x-1)}{(y-1)^2} + \frac{6}{(y-1)} \right]
 \end{aligned} \tag{13}$$

428 As for the case of pure aggregation, to solve the PBE with the LSPI
 429 method, the summations in equation 13 are transformed into integrals by
 430 means of the Euler-Maclaurin approximation:

$$\begin{aligned}
 \frac{df(x_i, t)}{dt} = & - f(x_i, t) \left[\frac{m_i(1)}{2} + \int_1^{x_{max}} m_i(y) dy + \frac{m_i(J)}{2} \right] \\
 & + \left[\frac{n_i(1)}{2} + \int_1^{\lfloor x_i/2 \rfloor} n_i(y) dy + \theta_{x_i} \frac{n_i(y_J)}{2} \right] \\
 & - \gamma(x_i) f(x_i, t) \\
 & + \left[\frac{p_i(1)}{2} + \int_{x_i+1}^{x_{max}} p_i(y) dy + \frac{p_i(J)}{2} \right]
 \end{aligned} \tag{14}$$

Breakage Parameters	Random	Mass	Erosion
$\beta(x, y)$	1	$(x^{1/3} + y^{1/3})^3$	$(x^{1/3} + y^{1/3})^3$
$\gamma(x), \forall x > 1$	$10^{-4}(x - 1)$	$0.1e^{0.01x}$	$2x^{0.5}$
C	2	2	0.5
$[x_{min}, x_{max}]$	$[1, 5 \times 10^3]$	$[1, 3 \times 10^3]$	$[1, 2 \times 10^3]$
Initial condition	$f(1, 0) = 1$ $f(x > 1, 0) = 0$	$f(1, 0) = 1$ $f(x > 1, 0) = 0$	$f(1, 0) = 1$ $f(x > 1, 0) = 0$
Simulated τ [-]	$[0 - 5000]$	$[0 - 80]$	$[0 - 80]$
I_C [-]	10	10	15
I [-]	25	60	30
J [-]	90	90	95

Table 3: Note that $\gamma(x)$ is defined only for $x > 1$, as primary particles are assumed not to break. A relative tolerance of 10^{-4} was used for all cases. The absolute tolerance was 10^{-20} for the random breakage and 10^{-15} otherwise. In all cases, the Matlab integrator “ode15s” has been used. I represent the total number of grid points including I_c . The analytical solution for random breakage [63] has been reported in ESI Section S3.

431 where $p_i(y)$ is the integrand function, for which the time-dependency has
432 been dropped for the sake of compactness:

$$p_i(y) = 2\Gamma(x_i, y)\gamma(y)f(y, t) \quad (15)$$

433 The PBE in equation 14 were solved for three different cases, a ran-
434 dom breakage kernel, a mass-dependent breakage, and a mass- and position-
435 dependent breakage with parabolic daughter distribution. The corresponding
436 kernels are reported in the ESI, Section S3, while the values of the kinetic
437 parameters employed are shown in Table 3. The results obtained with the
438 LSPI method were compared with analytical solutions (where available) or
439 with the numerical solution obtained with the aforementioned Gaussian basis
440 function approach.[52]

441 3.3.1. Random breakage

442 To test the LSPI approach in a simple breakage scenario, a random break-
443 age mechanism has been employed. In particular, $\gamma(x) = 10^{-4}(x - 1)$, indi-
444 cates that breakage may occur in any of the $x - 1$ contact points with the
445 same probability (assuming binary contact of primary particles). Note that
446 the more complex product of $\Gamma(x, y)\gamma(y)$ simplifies to 1 by using $C = 2$ and

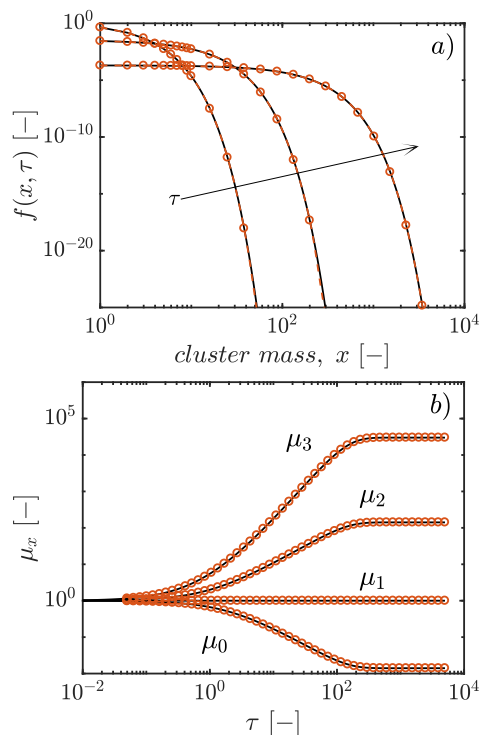


Figure 5: Discrete PBE for constant aggregation and breakage using the parameters reported in Table 3. Figure a) shows the distributions at non-dimensional times $\tau = 1, 10, 5000$ and b) the time-evolution of the moments of order $0^{th} - 3^{rd}$. The black lines represent the analytical solution [63], the red dashed lines and circles the results of the logarithmic shape-preserving interpolation (LSPI) method.

447 the above mentioned expression for $\gamma(y)$. For a constant aggregation mecha-
 448 nism and this simple breakage scheme an analytical solution exists.[63] Dis-
 449 tributed and average properties obtained with the LSPI method (red dashed
 450 lines and circles) have been compared with the analytical solutions (black
 451 solid lines) in Figure 5.

452 A perfect overlap of all properties can be observed when inspecting Fig-
 453 ure 5. Notably, $I = 25$ nodes and $J = 90$ knots were sufficient to obtain a
 454 very good overlap over more than 20 orders of magnitude for the distribu-
 455 tions (Figure 5 a)). The transition towards a stable stationary state where
 456 aggregation and breakage reach an equilibrium is well-captured by the LSPI
 457 method, as can be seen in Figure 5 b).

458 *3.3.2. Mass- and position-dependent breakage*

459 To test the LSPI approach with more complex breakage kernels, two lit-
460 erature cases (Table 3) were selected.[44] The first considered kernel is only
461 mass-dependent with $\gamma(x) = 0.1e^{0.01x}$, *i.e.* larger clusters break faster than
462 smaller ones. As in this first case, at $C = 2$, no position dependency arises
463 as $\Gamma(x, y)$ simplifies to 1 (equation 13 and ESI Section S3). The second ker-
464 nel is instead a mass- and position-dependent breakage kernel. In this latter
465 case larger clusters break easier than smaller ones (in fact $\gamma(x) = 2x^{0.5}$), and
466 breakage occurs more likely in the so-called “erosion” mode. This results
467 from using $C = 0.5$ in equation 13 and implies that the most favored break-
468 age events are those involving the “detachment” of smaller fragments (ESI,
469 Section S3). Given that no analytical solution exists for the above mentioned
470 kernels, a numerical comparison of the LSPI approach with the Gaussian ba-
471 sis function method has been performed. Both distributed (panels a) and
472 b)) and average properties (panels c) and d)) have been considered (Figure
473 6).

474 A perfect overlap of the two methods is observed in all cases. Despite the
475 more complex shape of the breakage kernels (Table 3 and ESI, Figures in Sec-
476 tion S3), the LSPI method requires some more grid points only when dealing
477 with the particularly stiff mass-dependent kernel. In any case, thanks to the
478 decoupling between number of elements and quadrature knots, the number
479 of grid points could be increased while keeping the same amount of inter-
480 polation knots as used in all other cases (Table 3). Moreover, it is worth
481 mentioning that the Gaussian basis function method requires 180 bases (and
482 a corresponding number of equations) in order to give satisfactory results.
483 This is due to the shape of the base function: given that a very abrupt
484 non-Gaussian distribution arises in the latter two cases, a high number of
485 Gaussian bases are necessary to well-approximate the shape of the distribu-
486 tion. The LSPI method suffers less from this problem, as it is defined on
487 finite elements, and because it deals with a shape-preserving interpolation of
488 the logarithm of $f(x, t)$. As a result, it is less sensitive to the shape of the
489 distribution and requires significantly less grid points and a corresponding
490 number of differential equations to give comparable results in terms of system
491 dynamics.

492 *3.4. Summary of discretized equations*

493 For the sake of clarity, a summary of the different terms required to solve
494 the PBE involving aggregation and breakage, for the continuous and for the

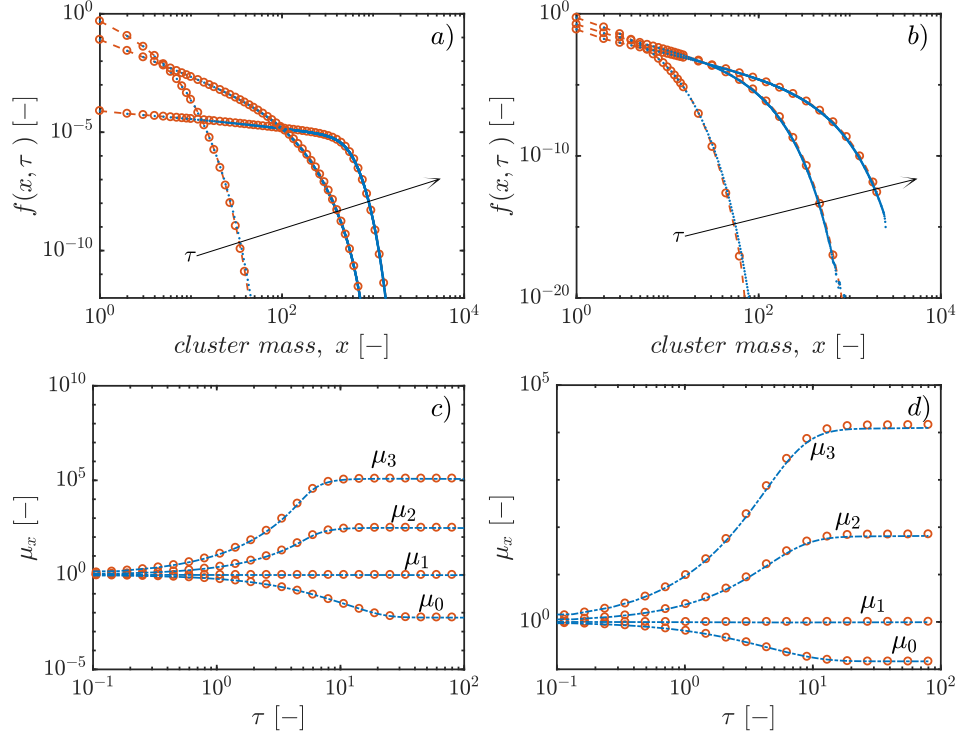


Figure 6: Discrete PBE for aggregation and breakage solved using the mass-dependent breakage (panels a) and c)), and the erosion breakage (panels b) and d)). Distributions are shown for $\tau = \{0.8, 4, 80\}$, and moments of order $0^{th} - 3^{rd}$ are reported. Blue dotted lines were obtained using the Gaussian basis functions (GBF) method, the red dashed lines and the circles are the solution of the logarithmic shape-preserving interpolation (LSPI) method.

495 discrete cases, is reported in Table 4. In both circumstances, the sum of
 496 the four terms is the time derivative $df(x_i, t)/dt$ at time t , which needs to
 497 be computed at each time integration step. It can be noticed the similarity
 498 between the two formulations, both involving three integrals (one for each
 499 grid point of coordinate x_i) to be evaluated by numerical quadrature. In
 500 practice, by means of the Euler-Maclaurin approximation, which allows to
 501 approximate a series with an integral, the discrete problem is also treated as
 502 a pseudo-continuous one. The main difference between the two cases relies
 503 on the need, when dealing with discrete problems, to add to each integral the
 504 sum of half the values of the integrand functions evaluated at the integration
 505 limits, as reported in Table 4. These additional terms are a consequence of
 506 the Euler-Maclaurin approximation (cf. Eq.6 and Eq.7) too. Note that, in
 507 the integral representing the rate of formation due to aggregation, when the
 508 domain of integration is halved (i.e. when integrating up to $x_i/2$ rather than
 509 up to $x_i - 1$ and than halving the result), the correction term for the upper
 510 limit of integration needs to be carried out only if x_i is odd.

511 4. Conclusions

512 In the present paper a new numerical approach to solve population bal-
 513 ance equations (PBE) has been introduced. The method relies on logarithmic
 514 shape-preserving interpolation (LSPI) on finite elements and falls in the so-
 515 called “basis functions” category. In the LSPI approach, the PBE are written
 516 for specific grid values and the integrals are evaluated by standard numeri-
 517 cal quadrature rules. Thus, the resulting system of differential equations is
 518 solved without further manipulation. The unknown, off-grid values of the
 519 distribution function required for the quadratures are calculated through in-
 520 terpolation from the known values at the grid points using shape-preserving
 521 piecewise cubic Hermite polynomials. To increase the efficiency of the in-
 522 terpolation, the logarithm of the distribution is interpolated rather than the
 523 distribution itself, given that in many cases distribution functions exhibit
 524 exponentially decaying tails.

525 After providing the theoretical foundation of the LSPI approach, the
 526 method has been tested in 8 different scenarios, dealing with aggregation
 527 and breakage mechanisms with both continuous and discrete PBE. In all
 528 cases the LSPI method performed very well, whether the comparison was
 529 made with distributed or averaged properties. Notably, a very small num-
 530 ber of differential equations were required in all cases, as low as 3-30, to

	continuous $f(x, t)$	discrete $f(x, t)$
domain of $f(x, t)$	$x_{min} \leq x \leq x_{max}$ with $x \in R \geq 0$	$1 \leq x \leq x_{max}$ with $x \in N$
rate of consumption of aggregates of size x_i due to aggregation	$-f(x_i, t) \int_{x_{min}}^{x_{max}} m_i(y) dy$	$-f(x_i, t) \left[\frac{m_i(1)}{2} + \int_1^{x_{max}} m_i(y) dy + \frac{m_i(y_J)}{2} \right]$
rate of formation of aggregates of size x_i due to aggregation	$\int_{x_{min}}^{x_i/2} n_i(y) dy$	$\frac{n_i(1)}{2} + \int_1^{\lfloor x_i/2 \rfloor} n_i(y) dy + \theta_{x_i} \frac{n_i(y_J)}{2}$
rate of consumption of aggregates of size x_i due to breakage	$-\gamma(x_i) f(x_i, t)$	$-\gamma(x_i) f(x_i, t)$
rate of formation of aggregates of size x_i due to breakage	$\int_{x_i}^{x_{max}} p_i(y) dy$	$\frac{p_i(1)}{2} + \int_{x_i+1}^{x_{max}} p_i(y) dy + \frac{p_i(y_J)}{2}$

Integrand and auxiliary functions

$$m_i(y) = \beta(x_i, y) f(y, t)$$

$$n_i(y) = \beta(x_i - y, y) f(x_i - y, t) f(y, t)$$

$$p_i(y) = 2\Gamma(x_i, y) \gamma(y) f(y, t)$$

$$\theta_{x_i} = 1 \text{ if } x_i \text{ is odd, } \theta_{x_i} = 0 \text{ if } x_i \text{ is even}$$

Table 4: Summary of the discretized equations for solving the PBE for the discrete and for the continuous cases. The functions β , γ and Γ represent the aggregation kernel, the breakage kernel and the daughter distribution function, respectively. For the sake of brevity, the explicit time dependency of the integrand functions, m_i , n_i and p_i , was omitted.

531 cover several order of magnitudes in both coordinates, with a single excep-
532 tion for a particularly stiff aggregation/breakage problem which required 60
533 grid points. A detailed analysis of the computational efficiency of the method
534 is outside the scope of the present work, but it is worth mentioning that all
535 simulations, carried out with Matlab on a basic desktop PC, required only a
536 few seconds down to fractions of a second, depending upon the problem at
537 hand, demonstrating the efficiency of the method. Undeniably, the compu-
538 tational power evens out many differences among methods, but a significant
539 number of advantages distinguish the LSPI approach from methods of the
540 same category:

- 541 • it is easy to apply as no residual needs to be calculated and no manip-
542 ulation of the original PBE is necessary;
- 543 • it provides accurate results with a limited number of finite elements/grid
544 points. This aspect is especially important in view of possible general-
545 izations to multidimensional cases;
- 546 • the number of grid points (*i.e.* of differential equations actually solved)
547 is decoupled from the number of interpolation points used to compute
548 the integrals, allowing to optimize the number of finite elements and
549 the quadrature knots independently.

550 Overall, several other steps will be necessary to prove the breadth and relia-
551 bility of the LSPI approach, such as employing it for nucleation and growth
552 problems and solving multidimensional PBE. Nevertheless, this work repre-
553 sents an important step towards the development of efficient interpolation-
554 based strategies to solve PBE.

555 5. Acknowledgments

556 S.L. gratefully acknowledges the Swiss National Science Foundation (SNSF)
557 for financial support (grant numbers P300P2_167683).

Table 5: List of Latin symbols

Parameter	Meaning	Units
b_i, c_i, d_i	interpolation parameter	—
C	parameter in breakage kernel	—
d_ϵ	shift factor parameter	—
D_p	particle diameter	m
E_μ	Error on first 4 moments	%
$f(x, t)dx$	number concentration of clusters with mass comprised between x and $x + \Delta x$	$\# L^{-1}$
h_i	length of i^{th} interval on the grid	—
I	number of grid points where the PBE are discretized	—
J	number of grid points used to interpolate $f(x, t)$ and compute the integrals of the PBE	—
k_B	Boltzmann constant	$J K^{-1}$
$m_i(y), n_i(y), p_i(y)$	function used in quadrature	—
$P(y, t)$	sought cubic interpolant	—
N_0	initial particle concentration	—
s	dissociation rate	s^{-1}
t	time	s
T	temperature	K
x, y	internal coordinate of the PBE	—
x_0	parameter for analytical solutions	—
x_i	i^{th} grid point where PBEs are solved where $i = 1, 2, \dots, I$	—
\underline{x}	vector containing x_i	—
x_{min}, x_{max}	smallest and largest cluster considered	—
y_j	j^{th} grid point used for quadratures where $j = 1, 2, \dots, J$	—
\underline{y}	vector containing y_i	—
w_j	weights used in quadrature	—
W	Fuchs stability factor	—

Table 6: List of Greek symbols

Parameter	Meaning	Units
$\beta(x, y)$	aggregation rate constant of an x - and a y -sized cluster	$m^3 \#^{-1} s^{-1}$
$\gamma(x)$	breakage rate of an x -sized cluster	$[s^{-1}]$
$\Gamma(x, y)$	probability that an x -sized cluster breaks in position y	$[-]$
δ_i	first divided difference on the i^{th} interval	$-$
Δ_i	segment width for quadratures	$-$
ϵ	shift factor	$-$
η	viscosity	$Pa\ s$
θ	parameter used for discrete PBE	$-$
λ	RLCA kernel parameter	$-$
$\mu_i(t)$	i^{th} moment of the distribution	$m^k \# L^{-1}$
$\mu_i^{an}(t)$	i^{th} moment of the distribution from analytical solutions	$m^k \# L^{-1}$
τ	non-dimensional time	$-$
ϕ	occupied volume fraction	$-$
ω_1, ω_2	parameters used in interpolation	$-$

559 7. References

- 560 [1] N. Hildebrandt, C. M. Spillmann, W. R. Algar, T. Pons, M. H. Stewart,
561 E. Oh, K. Susumu, S. A. Diaz, J. B. Delehanty, I. L. Medintz,
562 Energy transfer with semiconductor quantum dot bioconjugates: A ver-
563 satile platform for biosensing, energy harvesting, and other developing
564 applications, *Chemical Reviews* 117 (2017) 536–711. PMID: 27359326.
- 565 [2] I. Lignos, R. Maceiczkyk, A. J. deMello, *Microfluidic technology: Uncov-*
566 *ering the mechanisms of nanocrystal nucleation and growth*, *Accounts*
567 *of Chemical Research* 50 (2017) 1248–1257. PMID: 28467055.
- 568 [3] S. K. S. K. Friedlander, *Smoke, dust, and haze : fundamentals of aerosol*
569 *dynamics*, New York : Oxford University Press, 2nd ed edition, 2000.
570 Includes bibliographical references and index.
- 571 [4] D. Pfister, G. Storti, F. Tancini, L. Costa, M. Morbidelli, *Synthesis and*
572 *ring-opening polymerization of cyclic butylene 2,5-furandicarboxylate*,

- 573 Journal of Macromolecular Chemistry and Physics 216 (2015) 2141–
574 2146.
- 575 [5] L. Nicoud, M. Owczarz, P. Arosio, M. Morbidelli, A multiscale view of
576 therapeutic protein aggregation: A colloid science perspective, *Biotech-*
577 *nology Journal* 10 (2015) 367–378.
- 578 [6] S. Lazzari, L. Nicoud, B. Jaquet, M. Lattuada, M. Morbidelli, Fractal-
579 like structures in colloid science, *Advances in Colloid and Interface*
580 *Science* 235 (2016) 1–13.
- 581 [7] H. Hulburt, S. Katz, Some problems in particle technology, *Chemical*
582 *Engineering Science* 19 (1964) 555–574.
- 583 [8] D. Ramkrishna, *Population balances: Theory and applications to par-*
584 *ticulate systems in engineering*, 2000.
- 585 [9] N. Dotson, *Polymerization Process Modeling*, *Advances in interfacial*
586 *engineering series*, VCH, 1996.
- 587 [10] L. Costa, G. Storti, M. Morbidelli, L. Ferro, A. Galia, O. Scialdone,
588 G. Filardo, Copolymerization of vdf and hfp in supercritical carbon
589 dioxide: A robust approach for modeling precipitation and dispersion
590 kinetics, *Macromolecular Reaction Engineering* 6 (2012) 24–44.
- 591 [11] F. Teymour, J. D. Campbell, Analysis of the Dynamics of Gelation
592 in Polymerization Reactors Using the “Numerical Fractionation” Tech-
593 nique, *Macromolecules* 27 (1994) 2460–2469.
- 594 [12] Z. Chen, W. Pauer, H.-U. Moritz, J. Prss, H.-J. Warnecke, Modeling
595 of the suspension polymerization process using a particle population
596 balance, *Chemical Engineering & Technology* 22 (1999) 609–616.
- 597 [13] L. Costa, G. Storti, Kinetic modeling of precipitation and dispersion
598 polymerizations, *Advances in Polymer Science* - (2017) 1–33.
- 599 [14] H. Tobita, A. Hamielec, Modeling of network formation in free radical
600 polymerization, *Macromolecules* 3105 (1989) 3098–3105.
- 601 [15] A. Butté, G. Storti, M. Morbidelli, Evaluation of the Chain Length Dis-
602 tribution in Free-Radical Polymerization, 2. Emulsion Polymerization,
603 *Macromolecular Theory and Simulations* 11 (2002) 37–52.

- 604 [16] D. Meimaroglou, P. Pladis, A. Baltsas, C. Kiparissides, Prediction of
605 the molecular and polymer solution properties of ldpe in a high-pressure
606 tubular reactor using a novel monte carlo approach, *Chemical Engineer-*
607 *ing Science* 66 (2011) 1685 – 1696.
- 608 [17] L. Costa, G. Storti, M. Morbidelli, A. Galia, , G. Filardo, The rate
609 of polymerization in two loci reaction systems: Vdf-hfp precipitation
610 copolymerization in supercritical carbon dioxide, *Polymer Engineering*
611 *and Science* 51 (2011) 2093–2102.
- 612 [18] S. Lazzari, S. Hamzehlou, Y. Reyes, J. R. Leiza, M. R. P. Costa, R. Dias,
613 G. Storti, Bulk crosslinking copolymerization: comparison of different
614 modeling approaches, *Macromolecular Reaction Engineering* 8 (2014)
615 678–695.
- 616 [19] R. Pokorn, A. Zubov, P. Matuka, F. Lueth, W. Pauer, H.-U. Moritz,
617 J. Kosek, Process model for styrene and n-butyl acrylate emulsion
618 copolymerization in smart-scale tubular reactor, *Industrial & Engineer-*
619 *ing Chemistry Research* 55 (2016) 472–484.
- 620 [20] S. Hamzehlou, Y. Reyes, J. R. Leiza, Detailed microstructure investi-
621 gation of acrylate/methacrylate functional copolymers by kinetic monte
622 carlo simulation, *Macromolecular Reaction Engineering* 6 (2012) 319–
623 329.
- 624 [21] S. Hamzehlou, J. R. Leiza, J. M. Asua, A new approach for mathe-
625 matical modeling of the dynamic development of particle morphology,
626 *Chemical Engineering Journal* 304 (2016) 655 – 666.
- 627 [22] W. Koch, S. Friedlander, The effect of particle coalescence on the surface
628 area of a coagulating aerosol, *Journal of Colloid and Interface Science*
629 140 (1990) 419 – 427.
- 630 [23] P. T. Spicer, S. E. Pratsinis, Coagulation and fragmentation: Universal
631 steady-state particle-size distribution, *AIChE Journal* 42 (1996) 1612–
632 1620.
- 633 [24] P. Sandkühler, J. Sefcik, M. Lattuada, H. Wu, M. Morbidelli, Modeling
634 structure effects on aggregation kinetics in colloidal dispersions, *AIChE*
635 *journal* 49 (2003) 1542–1555.

- 636 [25] M. Soos, L. Wang, R. Fox, J. Sefcik, M. Morbidelli, Population balance
637 modeling of aggregation and breakage in turbulent taylorcouette flow,
638 Journal of Colloid and Interface Science 307 (2007) 433 – 446.
- 639 [26] M. Kostoglou, Extended cell average technique for the solution of co-
640 agulation equation, Journal of Colloid and Interface Science 306 (2007)
641 72 – 81.
- 642 [27] C. Kiparissides, A. Alexopoulos, A. Roussos, G. Dompazis, C. Kotoulas,
643 Population balance modeling of particulate polymerization processes,
644 Industrial and Engineering Chemistry Research 43 (2004) 7290–7302.
- 645 [28] D. L. Marchisio, R. O. Fox, Solution of population balance equations
646 using the direct quadrature method of moments, Journal of Aerosol
647 Science 36 (2005) 43 – 73.
- 648 [29] D. Kashchiev, Nucleation, Butterworth-Heinemann, 2000.
- 649 [30] J. Schöll, C. Lindenberg, L. Vicum, J. Brozio, M. Mazzotti, Precipi-
650 tation of α -glutamic acid: determination of growth kinetics, Faraday
651 Discussions 136 (2007) 247.
- 652 [31] M. Iggländ, M. Mazzotti, A population balance model for chiral res-
653 olution via Viedma ripening, Crystal Growth and Design 11 (2011)
654 4611–4622.
- 655 [32] D. Segets, M. A. Hartig, J. Gradl, W. Peukert, A population balance
656 model of quantum dot formation: Oriented growth and ripening of zno,
657 Chemical engineering science 70 (2012) 4–13.
- 658 [33] S. Lazzari, M. Abolhasani, K. F. Jensen, Modeling of the formation
659 kinetics and size distribution evolution of ii-vi quantum dots, Reaction
660 Chemistry & Engineering (2017).
- 661 [34] R. McGraw, S. Nemesure, S. E. Schwartz, Properties and evolution of
662 aerosols with size distributions having identical moments, Journal of
663 Aerosol Science 29 (1998) 761 – 772.
- 664 [35] D. Marchisio, R. Fox, Computational Models for Polydisperse Particu-
665 late and Multiphase Systems, Cambridge Series in Chemical Engineer-
666 ing, Cambridge University Press, 2013.

- 667 [36] L. Costa, U. Trommsdorff, Control strategy and comparison of tuning
668 methods for continuous lactide ring-opening polymerization, *Chemical*
669 *Engineering and Technology* 39 (2016) 2117–2125.
- 670 [37] M. Asteasuain, C. Sarmoria, A. Brandolin, Recovery of molecular weight
671 distributions from transformed domains. part i. application of pgf to
672 mass balances describing reactions involving free radicals, *Polymer* 43
673 (2002) 2513–2527.
- 674 [38] A. Brandolin, A. A. Balbuena, M. Asteasuain, Improved numerical
675 inversion methods for the recovery of bivariate distributions of polymer
676 properties from 2d probability generating function domains, *Computers*
677 *& Chemical Engineering* 94 (2016) 272–286.
- 678 [39] R. Gunawan, I. Fusman, R. D. Braatz, High resolution algorithms
679 for multidimensional population balance equations, *AIChE Journal* 50
680 (2004) 2738–2749.
- 681 [40] A. Mesbah, H. J. Kramer, A. E. Huesman, P. M. V. den Hof, A con-
682 trol oriented study on the numerical solution of the population balance
683 equation for crystallization processes, *Chemical Engineering Science* 64
684 (2009) 4262 – 4277.
- 685 [41] B. Szilgyi, Z. K. Nagy, Graphical processing unit (gpu) acceleration
686 for numerical solution of population balance models using high resolu-
687 tion finite volume algorithm, *Computers & Chemical Engineering* 91
688 (2016) 167 – 181. 12th International Symposium on Process Systems
689 Engineering & 25th European Symposium of Computer Aided Process
690 Engineering (PSE-2015/ESCAPE-25), 31 May - 4 June 2015, Copen-
691 hagen, Denmark.
- 692 [42] S. Kumar, D. Ramkrishna, On the solution of population balance equa-
693 tions by discretization - I. A fixed pivot technique, *Chemical Engineering*
694 *Science* 51 (1996) 1311–1332.
- 695 [43] M. Nicmanis, M. Hounslow, Finite-element methods for steady-state
696 population balance equations, *AICHE JOURNAL* 44 (1998) 2258–2272.
- 697 [44] M. Vanni, Approximate Population Balance Equations for Aggregation
698 and Breakage Processes, *Journal of Colloid and Interface Science* 221
699 (2000) 143–160.

- 700 [45] D. Bertin, I. Cotabarren, J. Pia, V. Bucal, Population balance dis-
701 cretization for growth, attrition, aggregation, breakage and nucleation,
702 *Computers & Chemical Engineering* 84 (2016) 132 – 150.
- 703 [46] S. Kumar, D. Ramkrishna, On the solution of population balance equa-
704 tions by discretization - II. A moving pivot technique, *Chemical Engi-
705 neering Science* 51 (1996) 1333 – 1342.
- 706 [47] J. Kumar, Numerical approximations of population balance equations
707 in particulate systems, Ph.D. thesis, Otto-von-Guericke-Universität
708 Magdeburg, Universitätsbibliothek, 2006.
- 709 [48] F. Gelbard, J. H. Seinfeld, Numerical solution of the dynamic equation
710 for particulate systems, *Journal of Computational Physics* 28 (1978)
711 357 – 375.
- 712 [49] S. Rigopoulos, A. Jones, Finite-element scheme for solution of the dy-
713 namic population balance equation, *AICHE JOURNAL* 49 (2003) 1127–
714 1139.
- 715 [50] M. Wulkow, Computer aided modeling of polymer reaction engineer-
716 ingthe status of predici, i-simulation, *Macromolecular Reaction Engi-
717 neering* 2 (2008) 461–494.
- 718 [51] A. M. Quarteroni, A. Valli, Numerical Approximation of Partial Differ-
719 ential Equations, Springer Publishing Company, Incorporated, 1st ed.
720 1994. 2nd printing edition, 2008.
- 721 [52] I. Kryven, P. D. Iedema, A Novel Approach to Population Balance Mod-
722 eling of Reactive Polymer Modification Leading to Branching, *Macro-
723 molecular Theory and Simulations* 22 (2013) 89–106.
- 724 [53] L. Gardini, A. Servida, M. Morbidelli, S. Carr, Use of orthogonal collo-
725 cation on finite elements with moving boundaries for fixed bed catalytic
726 reactor simulation, *Computers & Chemical Engineering* 9 (1985) 1–17.
- 727 [54] J. Solsvik, H. A. Jakobsen, Evaluation of weighted residual methods
728 for the solution of a population balance model describing bubbly flows:
729 The least-squares, Galerkin, tau, and orthogonal collocation methods,
730 *Industrial and Engineering Chemistry Research* 52 (2013) 15988–16013.

- 731 [55] D. Eyre, C. Wright, G. Reuter, Spline-collocation with adaptive mesh
732 grading for solving stochastic collection equation, *Journal of Computa-*
733 *tional Physics* 78 (1988) 288–304.
- 734 [56] N. Bellomo, B. Lods, R. Revelli, L. Ridolfi, *Generalized Collocation*
735 *Methods, Modeling and Simulation in Science, Engineering and Tech-*
736 *nology*, Birkhuser, 2008.
- 737 [57] F. N. Fritsch, R. E. Carlson, Monotone piecewise cubic interpolation,
738 *SIAM Journal on Numerical Analysis* 17 (1980) 238–246.
- 739 [58] C. Moler, *Numerical Computing with Matlab*, Society for Industrial and
740 *Applied Mathematics*, 2004.
- 741 [59] N. I. Lebovka, Aggregation of Charged Colloidal Particles, in: Muller,
742 M (Ed.), *POLYELECTROLYTE COMPLEXES IN THE DISPERSED*
743 *AND SOLID STATE I: PRINCIPLES AND THEORY*, volume 255 of
744 *Advances in Polymer Science*, 2014, pp. 57–96.
- 745 [60] S. C. Chapra, R. Canale, *Numerical Methods for Engineers*, McGraw-
746 *Hill, Inc.*, New York, NY, USA, 5 edition, 2006.
- 747 [61] I. Kryven, S. Lazzari, G. Storti, Population Balance Modeling of Aggre-
748 gation and Coalescence in Colloidal Systems, *Macromolecular Theory*
749 *and Simulations* 23 (2014) 170–181.
- 750 [62] S. Lazzari, B. Jaquet, L. Colonna, G. Storti, M. Lattuada, M. Morbidelli,
751 *Interplay between Aggregation and Coalescence of Polymeric Particles:*
752 *Experimental and Modeling Insights*, *Langmuir* 31 (2015) 9296–9305.
- 753 [63] P. J. Blatz, A. V. Tobolsky, Note on the kinetics of systems mani-
754 festing simultaneous polymerization-depolymerization phenomena, *The*
755 *Journal of Physical Chemistry* 49 (1945) 77–80.